Techniques to improve imaging through discrete scattering media

Sermsak Jaruwatanadilok, Akira Ishimaru, and Yasuo Kuga

Department of Electrical Engineering, Box 352500, University of Washington

Seattle, Washington, 98195

Abstract. Imaging through random media is an important problem with many applications including optical remote sensing and bio-optics. In this paper, we will investigate the applications of Radiative Transfer Equation (RTE) in optical imaging. In particular, we study off-axis intensity subtraction (OAIS) and cross-polarization intensity subtraction (CPIS) imaging techniques. These techniques were proposed as a new way to improve image quality. We show the effectiveness of these techniques in this paper. Also, we investigate a new imaging technique using the freqency modulate waves, i.e., the photon density waves. We analyze the characteristic of intensity and polarization of the photon density waves with different modulation frequencies. We solve the RTE for linearly and circularly polarized waves by discrete ordinates method. Using the numerical solutions to the RTE, we will show the conditions in which OAIS and CPIS are most effective. Moreover, continuous photon density waves exhibit a narrow angular spectrum with a lower level of incoherent component compared to regular continuous waves. Also, the shape of pulse photon density waves shows less effect of multiple scattering of the random media. These findings establish the possibility of using photon density waves for better imaging.

1. Introduction

In this paper, we consider the specific intensity of light waves and photon density waves propagating through a random medium, which can be characterized as randomly distributed discrete spherical particles in a homogeneous background. In nature, a similar situation can be observed in optical remote sensing thru clouds and fog. In our previous works, we have studied the polarized waves in discrete random media using the radiative transfer equation and obtained numerical solution using the discrete ordinates method for plane-wave incident cases [Ishimaru, 1993],[Ishimaru, 2001],[Kim, 2001],[Cheung, 1982]. Forward and backscattered specific intensities were calculated for linear and circular incident polarizations for both CW and pulse cases. However, our previous studies did not include the behavior of photon density waves and the application of RT for imaging purpose. In this paper, with some modification to the RT equations, we use the specific intensity obtained from RT to analyze the behavior of the photon density waves. Moreover, Solution to RT can be used to calculate the Point Spread Function (PSF) and evaluate different imaging techniques. Imaging through discrete scattering media must deal with the loss of image clarity due to scattering by particles. The coherent component, which provides a diffraction limited image, decreases exponentially as the optical depth increases. On the other hand, the incoherent component, which induces the blurring of the images, increases as the waves propagate deeper in scattering media [Moscoso, 2001]. PSF which is essentially a delta-function response of a medium, is commonly used as the measure of the performance of an imaging system.

There are techniques to improve the image quality, and most of them are based on the methods to reduce incoherent intensity from the total intensity. The simplest approach is to use a narrow field of view detector. Another approach is the off-axis intensity subtraction (OAIS) method which was experimentally investigated recently [Shimizu, 2000]. However, the detailed analysis of OASI has not been conducted yet. We will use our numerical models to investigate the effectiveness of OAIS and demonstrate that OAIS can show improvement in image quality. Polarization can also be used for reducing incoherent intensity [Demos, 1997]. In our previous paper [Ishimaru, 2001], we have

discussed that the cross-polarized component can be used for improving image quality. For a large optical depth, the level of cross-polarized component becomes comparable to that of the incoherent co-polarized component. Thus, by subtracting the cross-polarized component from co-polarized component, we can expect that the incoherent component in co-polarized light can be reduced. As a result, image quality can be improved. The behavior of photon density waves also suggests the possibility to be used to improve the imaging. It is shown that the photon density waves suffer less from multiple scattering effect. Thus, the images using photon density waves provide better quality.

In this paper, we will briefly discuss the pulse vector radiative transfer equation and its solution for linear and circular polarization in section 2. Details on this subject can be found in our previous paper [Ishimaru, 2001]. We will obtain PSF for a given imaging system in section 3 and the off-axis intensity subtraction and the cross-polarized intensity subtraction techniques will be studied in Section 4. Photon density waves are explained in Section 5. Section 6 is the conclusion.

2. Pulse Vector Radiative Transfer Equation and Its Solutions

We seek the solution for the narrow-band, time-dependent vector radiative transfer equations in a plane-parallel medium as shown in Fig.1. τ is the optical distance defined as $\tau = \rho\sigma_t z$ where ρ is the number density, σ_t is the total cross section of a single particle, and z is the actual distance. τ_o is the total optical depth defined by $\tau_o = \rho\sigma_t L$ where L is length of the random medium. The frequency-dependent vector radiative transfer equation for the diffuse component $\mathbf{I}_d$ is given by the following

$$\mu\frac{\partial}{\partial\tau}\mathbf{I}_d(\omega,\tau,\mu,\phi)+\left(1+(\mu-1)i\frac{\omega}{\tau_o}\right)\mathbf{I}_d(\omega,\tau,\mu,\phi)$$
$$=\int_0^{2\pi}\int_{-1}^{1}\mathbf{S}(\mu,\phi,\mu',\phi')\mathbf{I}_d(\omega,\tau,\mu',\phi')d\mu'd\phi'+\mathbf{F_o}(\tau,\mu,\phi)\exp(-\tau)\ \text{ for } 0\le\tau\le\tau_o \tag{1}$$

where $\mathbf{I}_d$ is a 4x1 modified Stokes vector.

The boundary conditions of $\mathbf{I}_d$ are

$$\mathbf{I}_d(\tau = 0) = 0 \qquad \text{for} \quad 0 \le \mu \le 1$$
$$\mathbf{I}_d(\tau = \tau_o) = 0 \qquad \text{for} \quad -1 \le \mu \le 0 \tag{2}$$

Physically, Eq. (2) shows that there is no diffuse intensity coming into the slab of random medium at the boundary. $\mu = cos\theta$ is the cosine of the polar angle, $\mathbf{F_o}$ is the 4x1 source term corresponding to the incident flux magnitude and **S** is the 4x4 Muller matrix. t is the normalized time given by [actual time / (L/c)] where c is the light speed in the medium. The time-dependent diffuse intensity can be calculated by applying a Fourier transform to the solution of the Eq. (1)

$$\mathbf{I}_d(t,\tau) = \frac{1}{2\pi}\int \mathbf{I}_d(\omega,\tau)\exp\left(i\frac{\omega}{\tau_o}\tau - i\omega t\right)d\omega \tag{3}$$

where $\mathbf{I}_d(t,\tau)$ is the modified Stokes vector in time-domain.

$$\mathbf{I}_d(t,\tau) = \left[I_1(t,\tau) \quad I_2(t,\tau) \quad U(t,\tau) \quad V(t,\tau)\right]^T \tag{4}$$

The total specific intensity is a sum of coherent (reduced) intensity $\mathbf{I}_{ri}$ and incoherent (diffused) intensity $\mathbf{I}_d$. The coherent intensity is expressed as

$$\mathbf{I}_{ri}(t,\tau) = \mathbf{I}_o \exp(-\tau)\delta(\phi)\delta(\mu - 1) \tag{5}$$

where $\mathbf{I}_o$ is the incident modified Stokes' parameter. We consider two cases of incident waves. Linear polarization in x-direction:

$$\mathbf{I}_o = \left[1 \quad 0 \quad 0 \quad 0\right]^T \tag{6}$$

Left-handed circular polarization:

$$\mathbf{I}_o = \left[1/2 \quad 1/2 \quad 0 \quad 1\right]^T \tag{7}$$

To obtain $\mathbf{I}_d$, we solve Eq. (1) with the boundary conditions stated in Eq. (2) using the discrete ordinates method [Ishimaru, 2001],[Cheung, 1982]. The discrete random medium is assumed to be dielectric spheres suspended in a homogeneous background for which the scattering characteristics can be obtained using the well known Mie solution [Van de Hulst, 1957]. For linear polarization, the co- and cross-polarized components in the forward direction are oriented in the *x*-direction and *y*-direction, respectively. On the other hand, for circular polarization, the co-polarized component in the forward

direction is left-handed and the cross-polarized component is right- handed. To solve equation (1), we expand the specific intensity in Fourier series. For linear polarization, the specific intensity is non-zero in mode zero and mode two, and for circular polarization, it is non zero only in mode zero. We also integrate the Muller matrix with respect to the ϕ dependence as expressed in Equation (8).

$$\mathbf{L}(\mu,\mu') = \int_0^{2\pi} \mathbf{S}(\mu,\mu',\phi'-\phi)d(\phi'-\phi) \tag{8}$$

As a result, Equation (1) reduce to

$$\begin{aligned} &\mu\frac{\partial}{\partial\tau}[\mathbf{I}_d(\omega,\tau,\mu)] + \left(1+(\mu-1)i\frac{\omega}{\tau_o}\right)[\mathbf{I}_d(\omega,\tau,\mu)] \\ &= \int_{-1}^{1} \mathbf{L}\ (\mu,\mu')][\mathbf{I}_d(\omega,\tau,\mu')]d\mu' + \mathbf{F}_o(\mu)\exp(-\tau) \quad \text{for } 0 \le \tau \le \tau_o \end{aligned} \tag{9}$$

By applying the Gauss quadrature formula in μ dependent to Equation (9), we obtain a first order differential equation in the form of

$$\frac{d}{d\tau}\mathbf{I} + \mathbf{A}\mathbf{I} = \mathbf{B}\exp(-\tau) \tag{10}$$

where

$$\mathbf{I} = \begin{bmatrix} \mathbf{I}_d(\omega,\tau,\mu_{-N}) \\ \vdots \\ \mathbf{I}_d(\omega,\tau,\mu_N) \end{bmatrix},\ \mathbf{A}_{j,k} = \frac{1}{\mu_j}\left(1+(\mu_j-1)i\frac{\omega}{\tau_o}\right) - \frac{\mathbf{L}(\mu_j,\mu_k)}{\mu_j}, \text{and } \mathbf{B}_{j,k} = \frac{\mathbf{F}_o(\mu_j)}{\mu_j} \tag{11}$$

The solution to equation (11) consists of the particular solution and the complementary solution. By imposing the boundary conditions in Equation (3), we can find the complete solution. We separately solve Equation (1) for linear polarization mode zero and mode two, and circular polarization mode zero. Table 1 shows the size distribution of fog used for numerical calculation throughout this paper.

3. Imaging System and Point Spread Function

Figure 2 shows the diagram of a simple imaging system that we used for our analysis. The circular lens has diameter of D with the focal distance of d_i. The field at the image plane is given by [Roggemann, 1996]

$$u_i(\bar{x}_i) = \frac{k^2}{(2\pi d_i)^2} \int u_o(\bar{x}) W_p(\bar{x}) \exp\left(i \frac{k}{2d_i} (\bar{x}_i^2 - 2\bar{x}_i \bar{x}) \right) dx \tag{12}$$

where the pupil aperture function $W_p(\bar{x})$ is 1 for $|\bar{x}| \le D/2$ and 0 for $|\bar{x}| > D/2$. $u_o(\bar{x})$ is the incident field on the lens. The intensity at the image plane is

$$I_i(\bar{x}_i) = \left\langle u_i(\bar{x}_i) u_i^*(\bar{x}_i) \right\rangle = \frac{k^2}{(2\pi d_i)^2} \iint \Gamma(\bar{x}_1, \bar{x}_2) W_p(\bar{x}_1) W_p(\bar{x}_2) \exp\left(-i \frac{k}{d_i} \bar{x}_i . (\bar{x}_1 - \bar{x}_2) \right) d\bar{x}_1 d\bar{x}_2 \tag{13}$$

With $\bar{x}_c = (\bar{x}_1 + \bar{x}_2)/2$ and $\bar{x}_d = \bar{x}_1 - \bar{x}_2$, and the assumption that $\Gamma(\bar{x}_1, \bar{x}_2) = \Gamma(\bar{x}_d)$, the Equation (13) becomes

$$I_i(\bar{x}_i) = \frac{k^2}{(2\pi d_i)^2} \iint \Gamma(\bar{x}_d) W_p(\bar{x}_1) W_p(\bar{x}_2) \exp\left(-i \frac{k}{d_i} \bar{x}_d \bar{x}_i \right) d\bar{x}_d d\bar{x}_c \tag{14}$$

where the mutual coherence function $\Gamma(\bar{x}_d)$ is given by

$$\Gamma(\bar{x}_d) = \int I_o(\bar{s}) \exp(ik\bar{s}\bar{x}_d) d\bar{s} \tag{15}$$

and $\bar{s} = \frac{\bar{x}}{d_i} = \sin\theta\cos\phi\ \hat{x} + \sin\theta\sin\phi\ \hat{y}$. The mutual coherence function consists of coherent and incoherent parts given by.

$$\begin{aligned} \Gamma_{coh}(\bar{x}_d) &= \int I_{o-coh}(\bar{s}) \exp(ik\bar{s}\bar{x}_d) d\bar{s} = \int I_o \exp(-\tau_o) \delta(\bar{s}) \exp(ik\bar{s}\bar{x}_d) d\bar{s} = e^{-\tau_o} \\ \Gamma_{inc}(\bar{x}_d) &= \int I_{o-inc}(\bar{s}) \exp(ik\bar{s}\bar{x}_d) d\bar{s} = \int I_d(\bar{s}) \exp(ik\bar{s}\bar{x}_d) d\bar{s} \end{aligned} \tag{16}$$

Substituting the Eq. (16) into (14), we have

$$I_i(\bar{x}_i) = I_{i-coh}(\bar{x}_i) + I_{i-inc}(\bar{x}_i) = \frac{k^2}{(2\pi d_i)^2} \left[e^{-\tau_o} A_i(k\bar{s}_i) + \int I_d(\bar{s}) A_i(k\bar{s}_i - k\bar{s}) d\bar{s} \right] \tag{17}$$

where the Airy pattern $A_i(k\bar{s}_i)$ is the point spread function of the imaging system given by

$$A_i(ks_i)=\left[\pi a^2 \frac{J_1(ks_i a)}{\frac{1}{2}ks_i a}\right]^2, \quad s_i=|\bar{s}_i| \tag{18}$$

From Eq. (17), we see that the specific intensity at the image plane is the combination of coherent intensity and incoherent intensity. The coherent component is the Airy pattern multiplied with a factor exponentially decreased by optical depth. On the other hand, the incoherent component is the convolution of diffuse intensity incident into the lens with the Airy pattern. One example of PSF of an imaging system is shown in Fig. 3. This is obtained using a circularly polarized light with λ=0.532 μm incident on a slab of fog particles. The lens diameter D=30 mm is used. The peak at S_i close to 0 is due to the coherent component which produces a diffraction limited image on the image plane. The incoherent component shows a broad angular spread which corresponds to a blurred image. As the optical depth increases, the difference between I_{coh} and I_{inc} becomes less thus the peak at S_i close to 0 decreases. Note that, in the figure, for optical depth of 30, the Airy pattern disappears because the incoherent intensity has larger magnitude than the coherent one. For a conventional imaging system, it is well known that the image quality is mainly determined by a relative magnitude of coherent and incoherent intensities at the image plane. We define the critical optical depth at which the values of I_{coh} and I_{inc} become equal, and the results are shown in Fig.4 as a function of aperture size D for 3 different wavelengths. As expected, the large aperture size which produces a narrow Airy pattern, captures the lesser amount of the incoherent intensity. Therefore, it produces a better image at large τ.

4. Off-axis intensity subtraction and cross-polarization intensity subtraction

To improve the image quality in optical remote sensing, different techniques have been investigated in the past, but most of them are based on the experimental approach. Although some of them show the improved results, it is difficult to generalize a specific experiment for other cases. In this section, therefore, we will numerically test two image enhancement techniques. Those are off-

axis intensity subtraction (OAIS) and cross-polarization intensity subtraction (CPIS) methods. OAIS is based on the fact that the off-axis (45degrees) intensity is mostly incoherent and the angular distribution is usually given by a $cos\theta$ pattern (Rambercian). Therefore, if we can estimate the incoherent intensity at θ=0 and subtract it from the total intensity, the coherent intensity can effectively be enhanced. CPIS is based on the fact that cross-pol intensity which is incoherent increases as τ becomes large. For a very large τ, the intensity of cross-pol is comparable to that of co-pol. This implies that if we can estimate the level of incoherent intensity based on the cross-pol value, we can effectively subtract the incoherent intensity from the total intensity.

We will test OAIS and CPIS for different cases. First we define the image contrast as

$$C = \frac{I_{i-coh}(s_i = 0) - I_{i-inc}(s_i = 0)}{I_{i-inc}(s_i = 0)} \tag{19}$$

Figures 5 (A) and (B) show the OAIS contrast in dB for the circularly- and linearly-polarized light, respectively. The contrast is shown for three cases: (1) based on only co-polarization component, (2) based on co-polarization component with off-axis subtraction (OAIS), and (3) based on the co-polarization component with cross-polarization subtraction (CPIS). From Figures 5, we conclude that OAIS produces a better result when the optical depth is small. Also, it appears that the contrast improvement of OAIS over the co-polarization only is almost independent of the optical depth. For large optical depth, CPIS performs better because the cross-polarization component increases as the optical depth becomes large.

Figure 6 (A) shows data with and without CPIS for linear and circular polarizations. The CPIS technique is effective for the linear polarization imaging because a linearly polarization light tends to lose its energy to the cross-polarization component faster than the circular polarization light as the optical depth increases. On the other hand, there is no difference between linear and circular polarization when using OAIS as shown in Fig. 6 (B).

5. Photon Density Radiative Transfer Equation and its solutions

The frequency-dependent vector radiative transfer equation for diffuse photon density waves with modulation frequency f_{mod} is given by the following

$$\mu\frac{\partial}{\partial\tau}\mathbf{I}_d(\omega,\tau,\mu,\phi)+\left(1+(\mu-1)i\frac{\omega+\omega_{\mathrm{mod}}}{\tau_o}\right)\mathbf{I}_d(\omega,\tau,\mu,\phi) = \int_0^{2\pi}\int_{-1}^{1}[\mathbf{S}(\mu,\phi,\mu',\phi')\mathbf{I}_d(\omega,\tau,\mu',\phi')]d\mu'd\phi'+\mathbf{F_o}(\tau,\mu,\phi)\exp(-\tau)\ \text{ for } 0\le\tau\le\tau_{\mathrm{o}} \tag{20}$$

where the normalized modulation frequency ω_{mod} is

$$\omega_{\mathrm{mod}}=\frac{2\pi f_{\mathrm{mod}}L}{c} \tag{21}$$

The boundary conditions of $\mathbf{I}_d$ are the same as Eq. (2). The time-dependent diffuse intensity can be calculated by applying a Fourier transform to the solution of the Equation (20)

$$\mathbf{I}_d(t,\tau)=\frac{1}{2\pi}\int\mathbf{I}_d(\omega,\tau)\quad\exp\left(i\frac{\omega+\omega_{\mathrm{mod}}}{\tau_o}\tau-i\omega t\right)d\omega \tag{22}$$

the procedures to solve for solutions are similar to those of plane waves explained in section 2. We use the wavelength of 1 micron. The random medium is fog particles with size distribution shown in Table 1 suspended in air. The path length of the medium (L) is 1 km. Concentration of fog particles is varied according to the optical depth. The following are the results obtained from numerical solutions

5.1 effects of modulation frequency on the diffused intensity

Figure 7 shows the angular spectrum of the continuous wave compared to photon density wave with different modulation frequencies. We notice that, for co-polarized component, as the modulation frequency increases, the angular spectrum sharpens and the level of intensity reduces. In the case of co-polarized component, the difference between linear and circular polarization is not pronounced. On the other hand, the figures look different between the cross-polarized components.

Figure 8 shows the forward intensity (at the angle of 0.68 degrees) comparing different modulation frequencies as a function of optical depth. For larger modulation frequency, the co-polarized intensity reduces much more rapidly when optical depth increases. Instead of increasing and

saturating as in the case of regular continuous wave, the cross-polarized intensity also decreases as optical depth increases.

5.2 effects of modulation frequency to the polarization characteristics

We consider the Degree Of Polarization (DOP) and the Cross (X) Polarization Discrimination (XPD) defined by Equation (23) and (24), respectively.

$$\mathrm{DOP\ (dB)} = 10\log\left[\frac{\sqrt{(I_1 - I_2)^2 + U^2 + V^2}}{I_1 + I_2}\right] \tag{24}$$

$$\mathrm{XPD\ (dB)} = 10\log\left[\frac{I_{co\text{-}pol}}{I_{x\text{-}pol}}\right] \tag{25}$$

Figure 9 shows the forward (0.68 degrees) DOP and XPD as functions of optical depth. We notice that the photon density waves with higher modulation frequency maintain their DOP even when optical depth increases. This suggests that photon density waves are less susceptible to change their polarization state in the multiple scattering environments. Also, the XPD of photon density waves is higher than that of CW.

5.3 the pulse photon density waves

Pulse photon density waves in random media have been solved. Figure 10 shows pulse shapes of linearly and circularly polarized waves and photon density waves as functions of time and angle. It is shown that pulse photon density waves maintain the shape of the original input pulse while the regular pulse waves shows some pulse broadening.

To visually illustrate the effectiveness of OAIS , CPIS, and photon density waves, we conduct numerical simulations using an image of a cross pattern. A cross pattern is imaged through random media. The angular size of object is equivalent to a cross with 6 mm by 6 mm with the thickness of 2 mm and spatial pixel size of 1 mm. The circular lens has a 30 mm aperture size and wavelength is 0.532 micron. The path length of random medium is 10 cm. The number density of particles is

adjusted to give the optical depth of 25. The images obtained using different techniques are shown in Figures 11 and 12.

Figure 11 shows the cross images with circularly polarized light of (A) the original cross image, (B) the cross image through the random medium using co-polarized waves, (C) the cross image through the random medium using OAIS, and (D) the cross image through the random medium using CPIS. Figure 12 shows the same cases for the linearly polarized light. The image contrast of these images is computed using Eq. (19) and listed in Table 2. From the results, it seems that a linearly polarized light with CPIS technique gives the best image contrast for this configuration. As we discussed earlier, the image contrast depends on τ, and OAIS generally provide a better image for small optical depth.

6. Conclusions

We have investigated the applications of radiative transfer equation in optical imaging. We derived the coherent and incoherent intensities at the image plane and they were expressed as the convolution of intensity with the Airy pattern of the lens. We have shown that the incoherent intensity is responsible for the degradation of image quality. The performance of the imaging techniques has been studies for a wide range of optical depth. Both OAIS and CPIS show improvement over the traditional approach. However, we found that OAIS is better suited for small optical depth whereas CPIS is more effective for large optical depth. We also found that the incident light must be linearly polarized to maximize the effectiveness of CPIS.

Polarization characteristics in terms of degree of polarization and cross polarization discrimination for photon density waves are examined. We found that generally photon density waves have lower level of incoherent intensity. Modulation frequency strongly affects on the angular spectrum and the level of intensity. Polarization characteristics also change drastically. Cross-polarization discrimination improves tremendously compared to the regular waves. Also, the pulse

shape of photon density waves shows less effect from multiple scattering compared to that of regular pulse waves. These results suggest the possibility of using photon density waves to get better images.

Acknowledgements. This work is supported by the National Science Foundation, the Office of Naval Research and the Air Force Research Laboratory. We thank Arnold D. Kim for his early work on pulse vector radiative transfer. Also, we thank Dr. Charles Matson, AFRL, for many discussion, comments and suggestions.

References

Bruscaglioni, P., G. Zaccanti, and Q. Wei, "Transmission of a pulsed polarized light beam through thick turbid media: numerical results," *Applied Optics*, Vol. 32, No. 30, pp.6142-6150, 1993.

Cheung, R. L-T and A. Ishimaru, "Transmission backscattering and depolarization of waves in randomly distributed spherical particles," *Applied Optics*, Vol. 21, pp. 3792-3798, 1982.

Demos, S. G. and R.R. Alfano, "Optical polarization imaging," *Applied Optics*, Vol. 36, pp. 150-155, 1997.

Kim, A. D., S. Jaruwatanadilok, A. Ishimaru, and Y. Kuga, "Polarized light propagation and scattering in random media," *to appear in SPIE*, Vol. 4257-A, 2001.

Moscoso, M., J. B. Keller, and G.C. Papanicolaou, "Depolarization and blurring of optical images by biological tissues," *Journal of Optical Society of America*. Vol. 18, No.4, pp. 948-60, 2001.

Ishimaru, A., *Wave Propagation and Scattering in Random Media*, IEEE Press, New York, 1997.

Ishimaru, A., S. Jaruwatanadilok, and Y. Kuga, "Polarized Pulse Waves in Random Discrete Scatterers," *Accepted for Applied Optic*, 2001.

Roggemann, M.C., and B. Welsh, *Imaging Through Turbulence*, CRC Press, New York, 1996.

Shimizu, K., and M. Kitama, "Fundamental Study on Near-Axis Scattered Light and Its Application to Optical Computed Tomography," *Optical Review*, Vol. 7, No. 5, pp. 383-388, 2000.

Van de Hulst, H. C., *Light Scattering by Small Particles*, Wiley, New York, 1957.

Table 1. Particle size distribution of fog

Diameter (microns)	0.4	0.6	0.7	1.4	2	3.6	5.4	8
Number of particles	3	10	40	50	7	1	9	2

Table 2. Contrast of the cross images

	Co-polarization	OAIS	CPIS	Photon density
Linear polarization	-0.7983	0.3338	5.4791	10.4949
Circular polarization	-0.8050	0.2754	1.0216	10.6349

LIST OF FIGURES

medium using CPIS, and E) 5 GHz photon density wave.

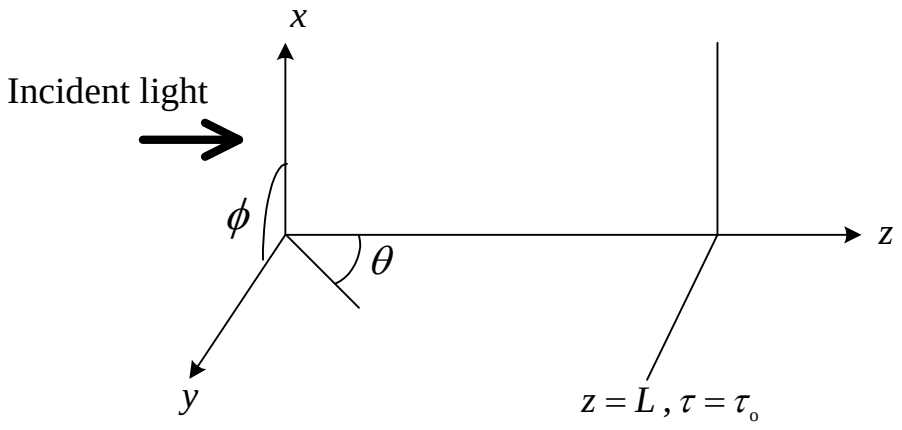

Figure 1. Plane parallel problem

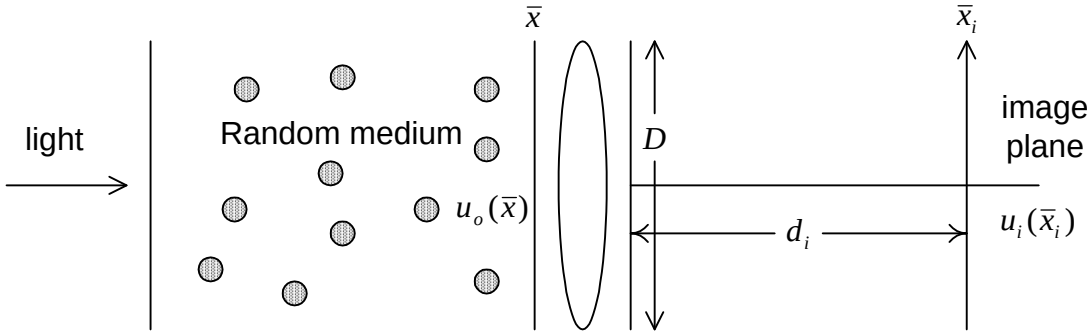

Figure 2. Imaging system

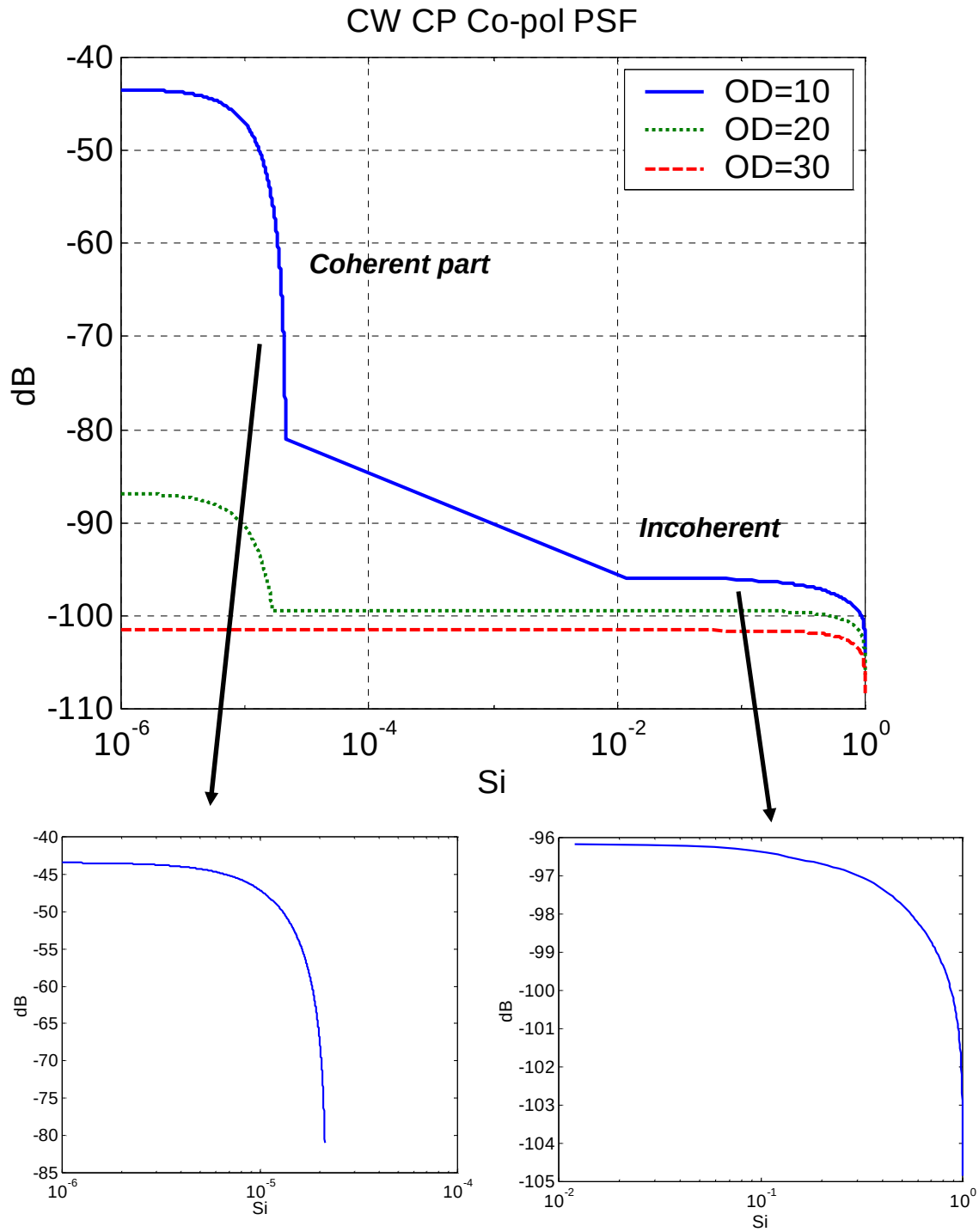

Figure 3. An example of PSF of an imaging system

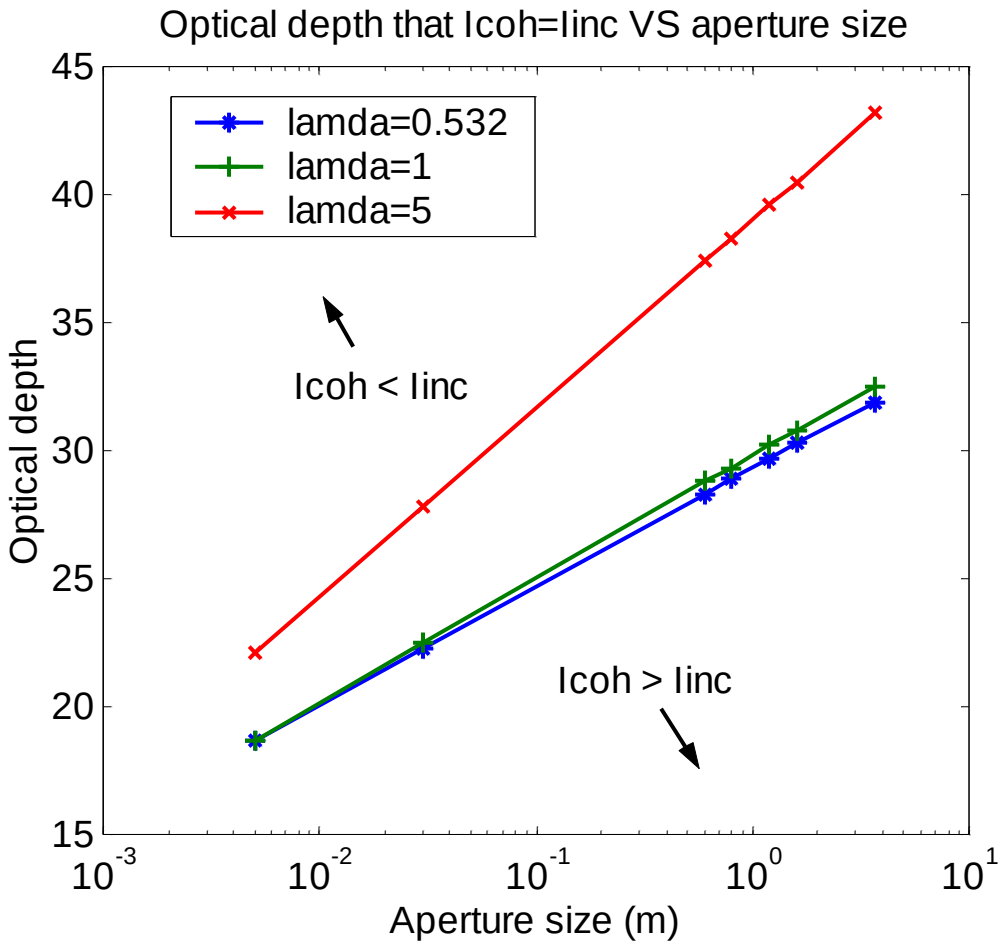

Figure 4. Plot of coherent equals to incoherent VS the optical depth and aperture size

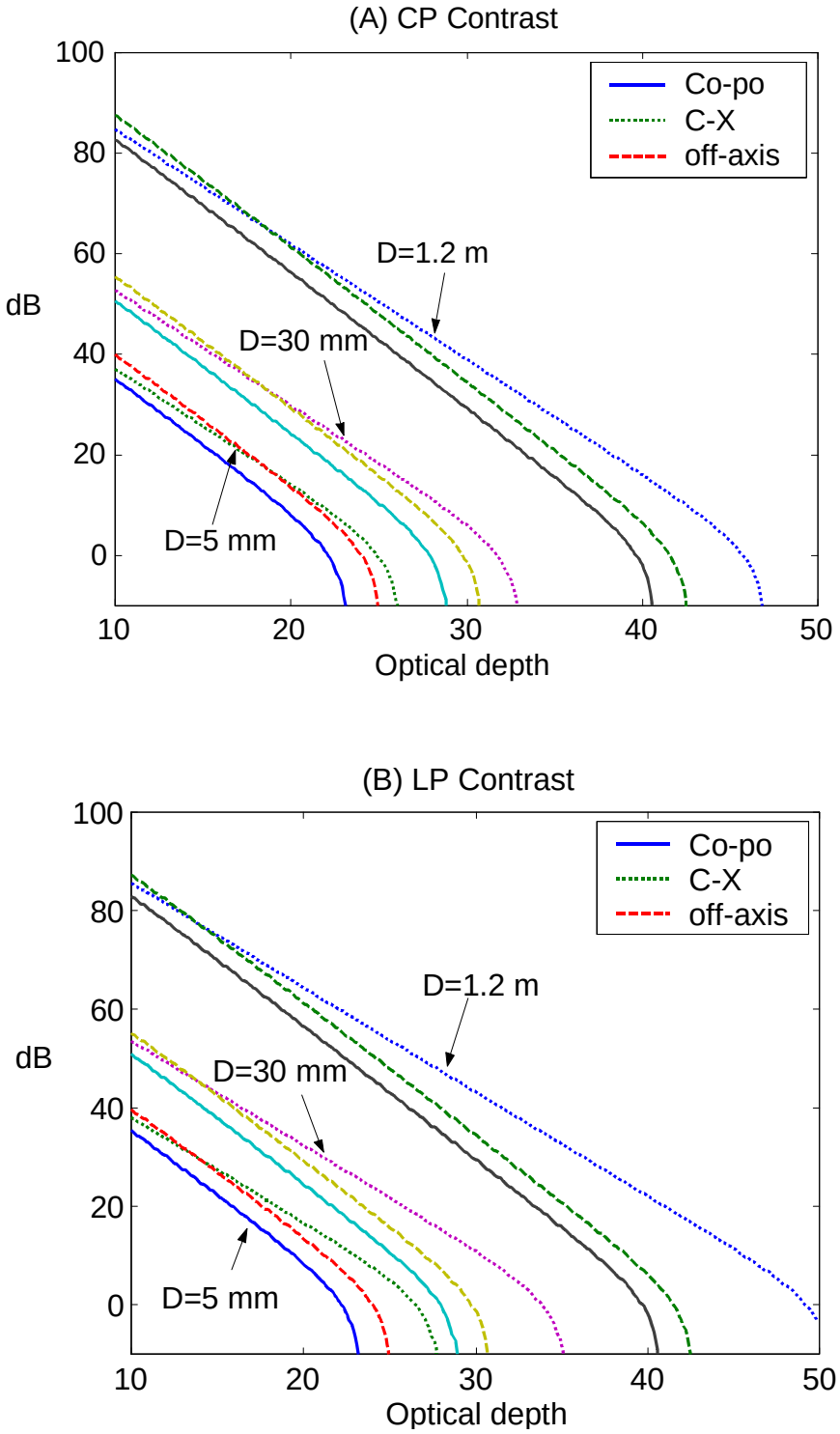

Figure 5. Contrast for (A) circular polarization, (B) linear polarization

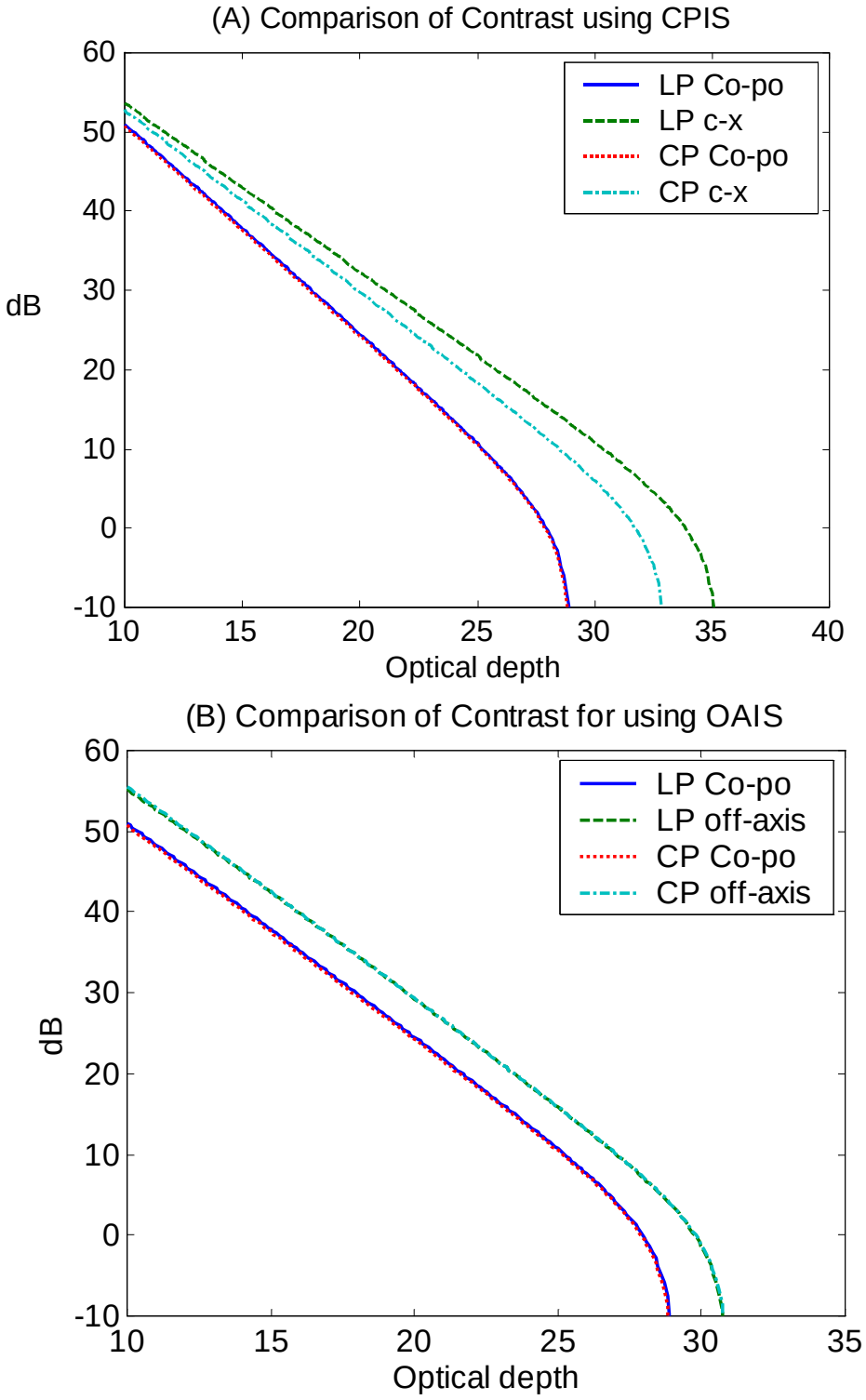

Figure 6. Comparison of linear and circular polarization using (A) cross-polarization subtraction (CPIS), (B) off-axis subtraction (OAIS)

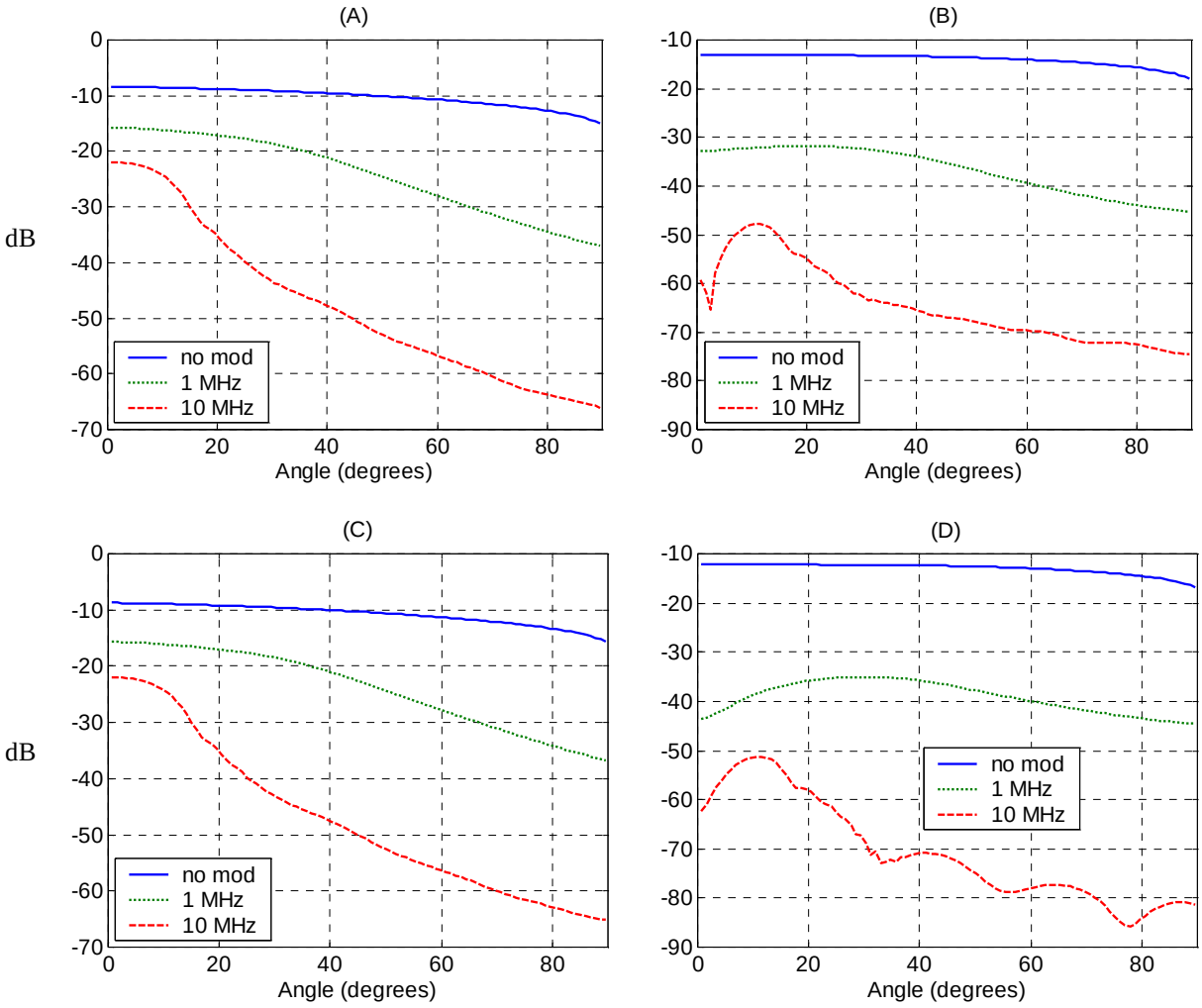

Figure 7. Angular spectrum of diffuse intensity of CW photon density waves at optical depth of 10 with different modulation frequencies A) Circular co-polarization, B) Circular cross polarization, C) Linear co-polarization, and D) Linear cross-polarization.

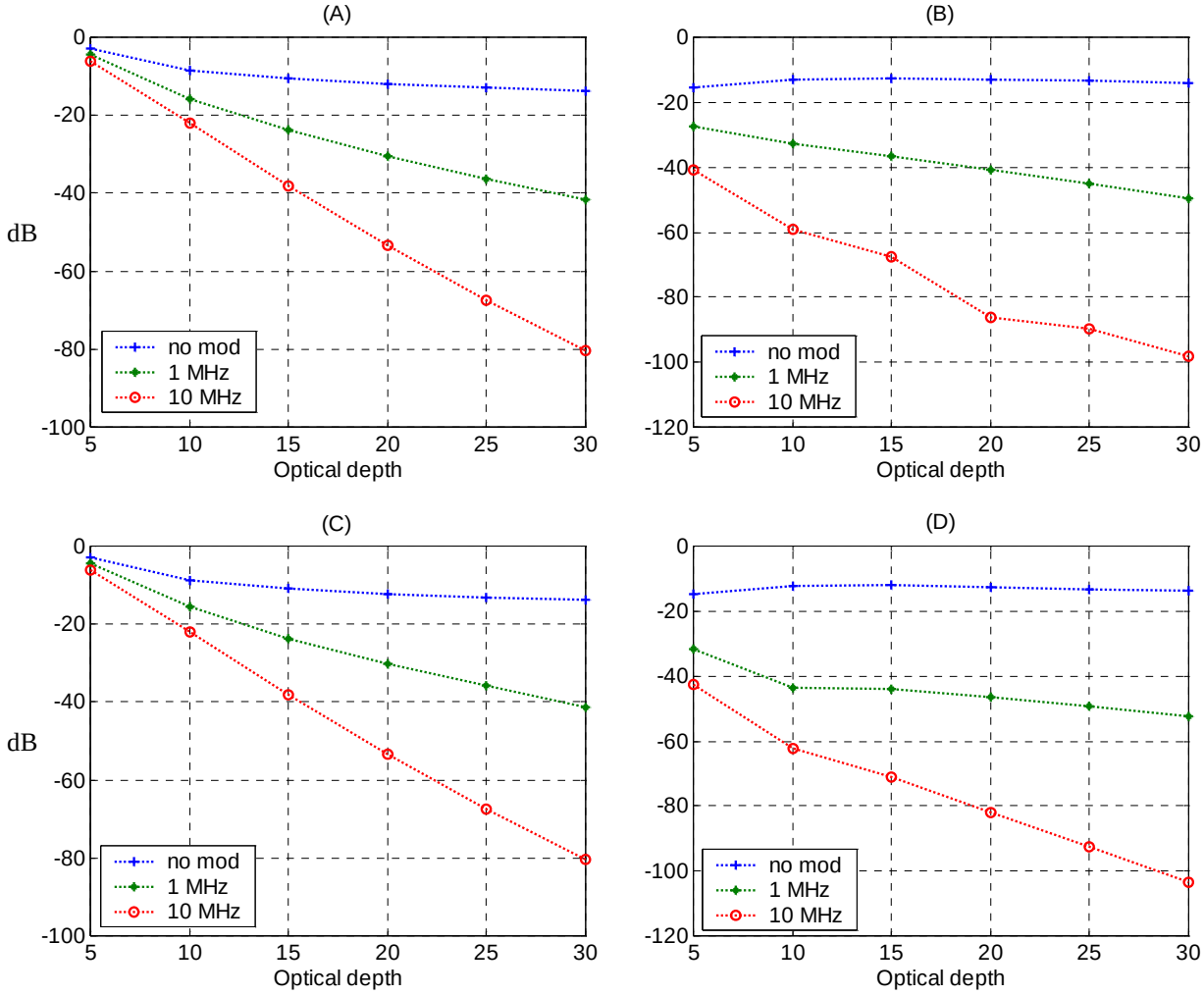

Figure 8. Diffused intensity of CW photon density waves with different modulation frequencies as a function of optical depth A) Circular co-polarization, B) Circular cross-polarization, C) Linear co-polarization, and D) Linear cross-polarization.

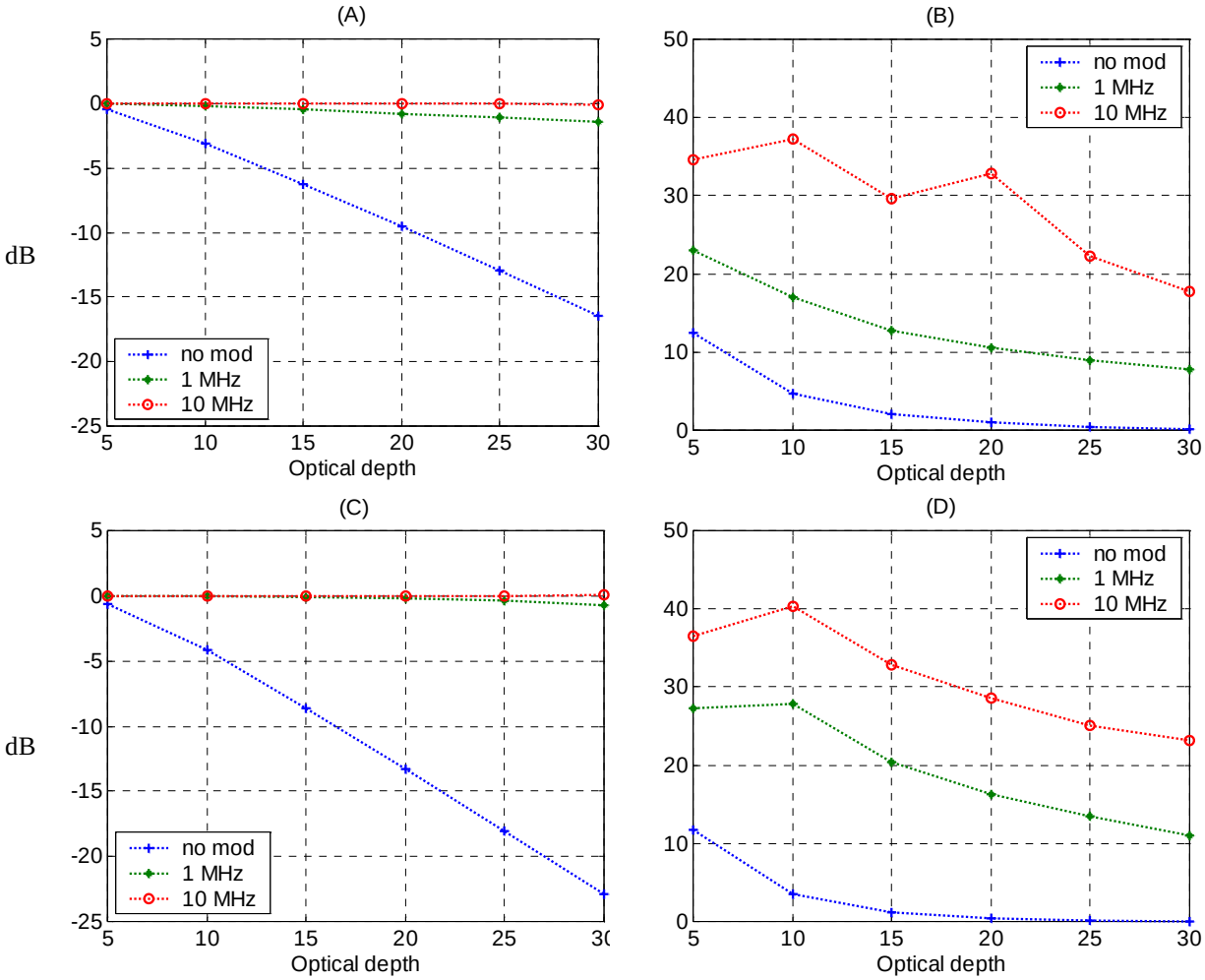

Figure 9. Polarization characteristic of photon density waves with different modulation frequencies as functions of optical depth A) DOP of circular polarization, B) XPD of circular polarization, C) DOP of linear polarization, and D) XPD of linear polarization

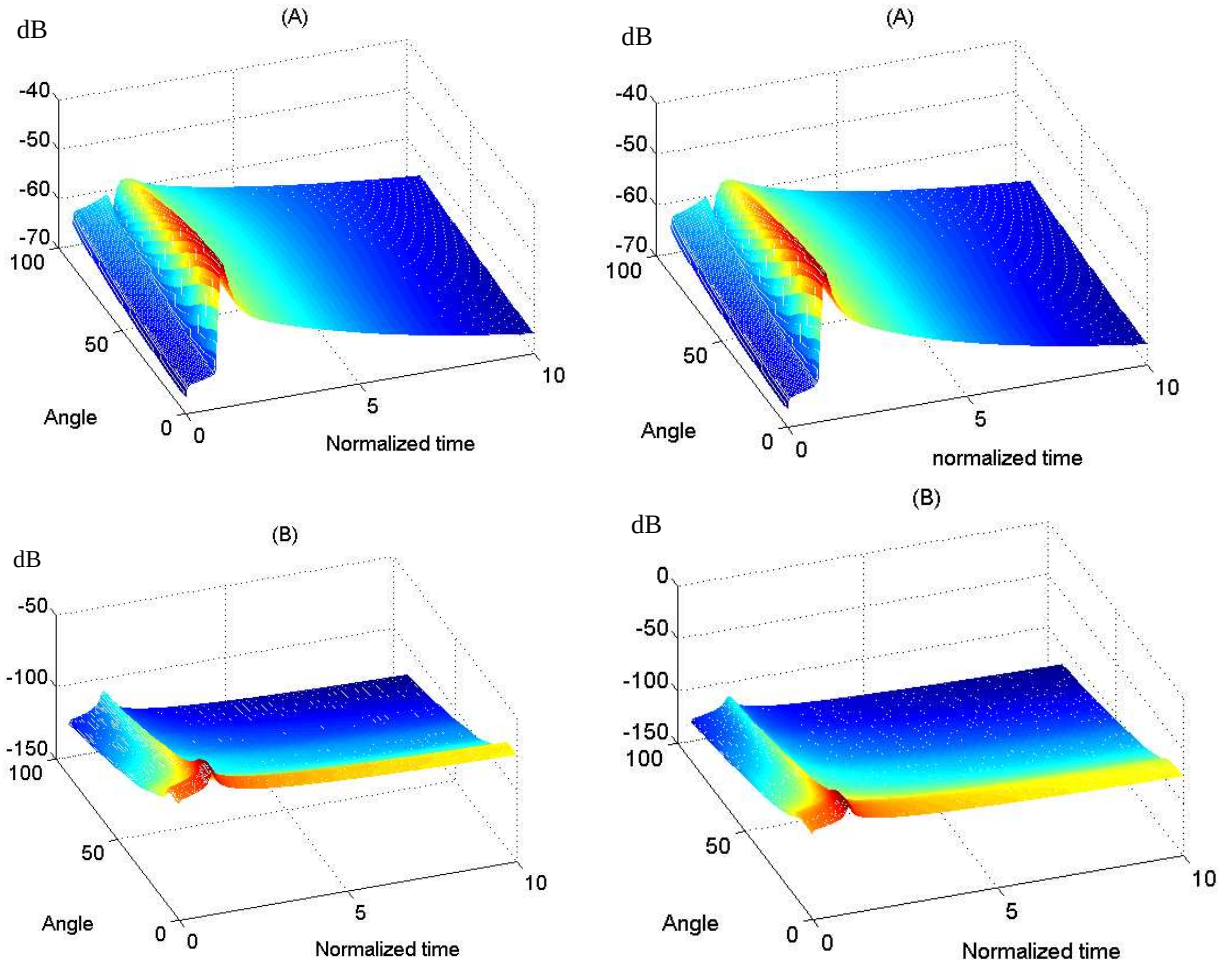

Figure 10. (LEFT) Linear co-polarized incoherent intensity (RIGHT) Circular co-polarized incoherent intensity (decibel) of (A) pulse waves and (B) pulse photon density waves with 10 MHz modulation.

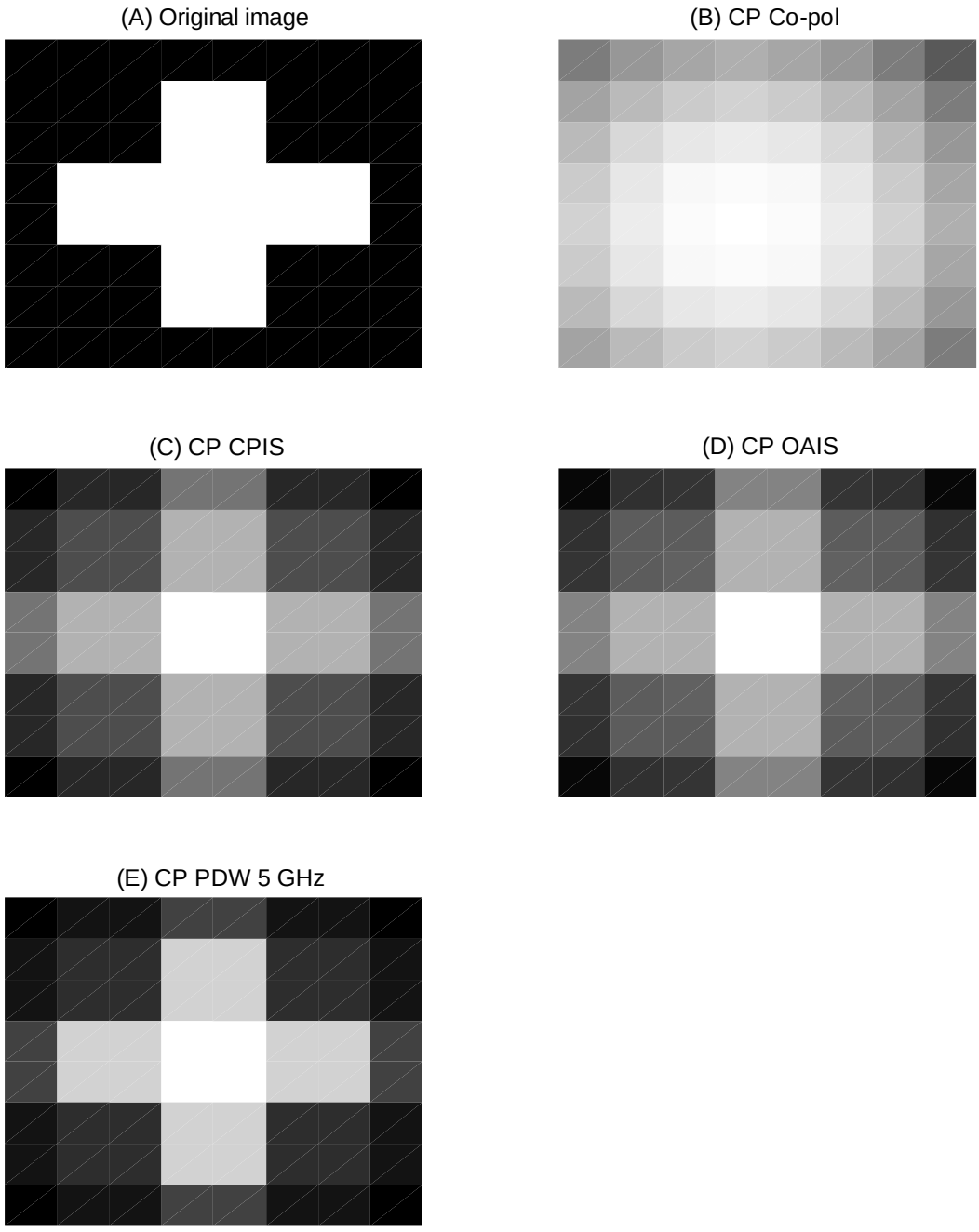

Figure 11. The circular polarized cross image A) the original, B) through random medium using co-polarized wave imaging, C) through random medium using off-axis subtraction, D) through random medium using CPIS, and E) 5 GHz photon density wave.

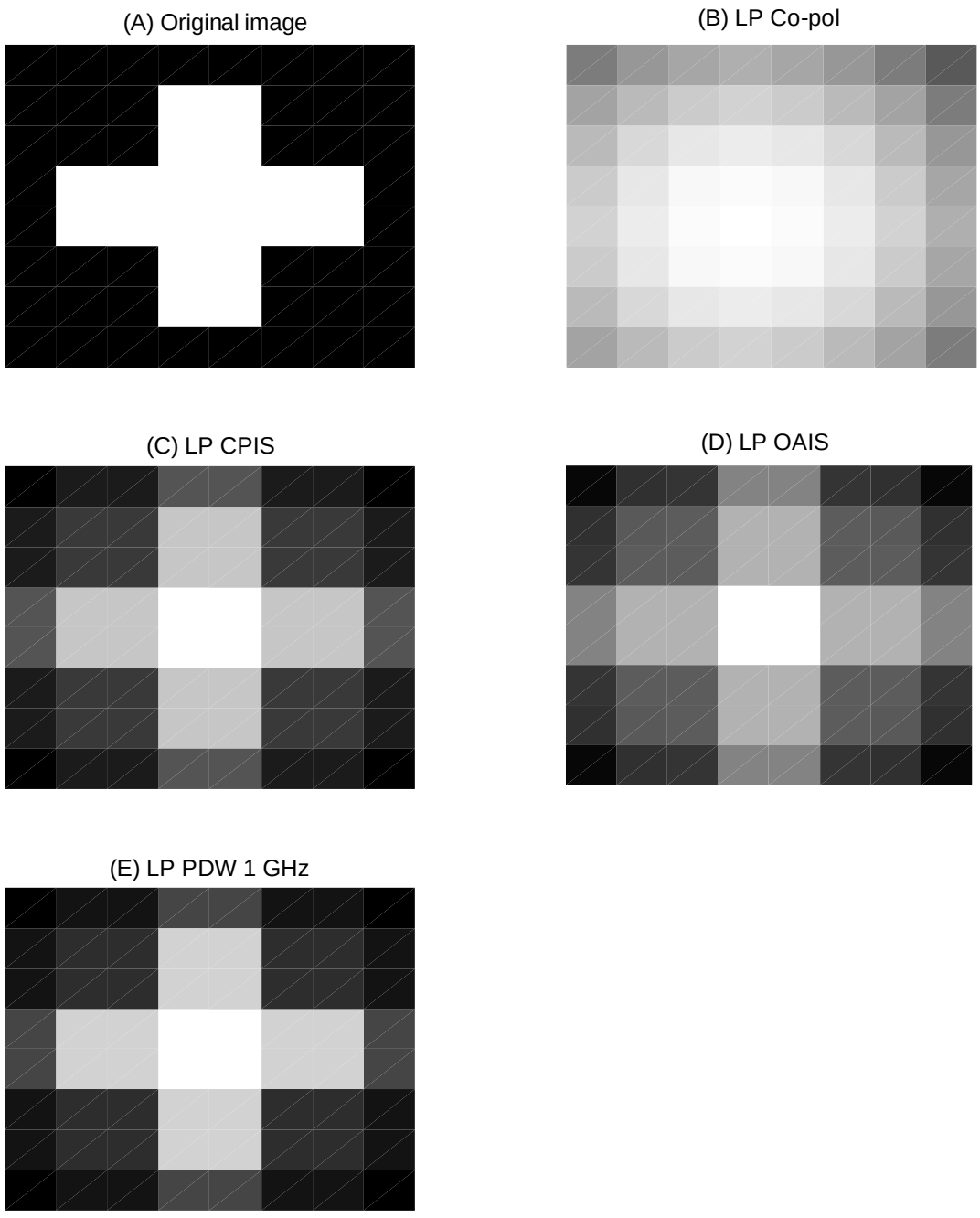

Figure 12. The linear polarized cross image A) the original, B) through random medium using co polarized wave imaging, C) through random medium using OAIS, D) through random medium using CPIS, and E) 5 GHz photon density wave.